

## PDF hosted at the Radboud Repository of the Radboud University Nijmegen

The following full text is a preprint version which may differ from the publisher's version.

For additional information about this publication click this link.

<http://hdl.handle.net/2066/155816>

Please be advised that this information was generated on 2017-12-05 and may be subject to change.

# Hubble Tarantula Treasury Project. IV. The extinction law<sup>\*</sup>

Guido De Marchi<sup>1</sup>, Nino Panagia<sup>2,3,4</sup>, Elena Sabbi<sup>2</sup>, Daniel Lennon<sup>5</sup>, Jay Anderson<sup>2</sup>,  
 Roeland van der Marel<sup>2</sup>, Michele Cignoni<sup>2</sup>, Eva K. Grebel<sup>6</sup>, Søren Larsen<sup>7</sup>,  
 Dennis Zaritsky<sup>8</sup>, Peter Zeidler<sup>6</sup>, Dimitrios Gouliermis<sup>9</sup>, Alessandra Aloisi<sup>2</sup>

<sup>1</sup>European Space Research and Technology Centre, Keplerlaan 1, 2200 AG Noordwijk, The Netherlands, [gdemarchi@esa.int](mailto:gdemarchi@esa.int)

<sup>2</sup>Space Telescope Science Institute, 3700 San Martin Drive, Baltimore, MD 21218, USA

<sup>3</sup>INAF–NA, Osservatorio Astronomico di Capodimonte, Salita Moiariello 16, 80131 Naples, Italy

<sup>4</sup>Supernova Ltd, OYV #131, Northsound Rd., Virgin Gorda VG1150, Virgin Islands, UK

<sup>5</sup>European Space Astronomy Centre, Apdo. de Correo 78, 28691 Villanueva de la Cañada, Madrid, Spain

<sup>6</sup>Astronomisches Rechen-Institut, Zentrum für Astronomie der Universität Heidelberg, Mönchhofstr. 12–14, 69120 Heidelberg, Germany

<sup>7</sup>Department of Astrophysics, Radboud University, P.O. Box 9010, 6500 GL Nijmegen, The Netherlands

<sup>8</sup>Steward Observatory, University of Arizona, 933 N. Cherry Ave, Tucson, AZ 85721-0065, USA

<sup>9</sup>Institut für Theoretische Astrophysik, Zentrum für Astronomie der Universität Heidelberg, Albert-Ueberle-Str. 2, 69120 Heidelberg, Germany

Received 1.9.2015; Accepted 27.10.2015

## ABSTRACT

We report on the study of interstellar extinction across the Tarantula nebula (30 Doradus), in the Large Magellanic Cloud, using observations from the Hubble Tarantula Treasury Project in the 0.3 – 1.6  $\mu\text{m}$  range. The considerable and patchy extinction inside the nebula causes about 3 500 red clump stars to be scattered along the reddening vector in the colour–magnitude diagrams, thereby allowing an accurate determination of the reddening slope in all bands. The measured slope of the reddening vector is remarkably steeper in all bands than in the Galactic diffuse interstellar medium. At optical wavelengths, the larger ratio of total-to-selective extinction, namely  $R_V = 4.5 \pm 0.2$ , implies the presence of a grey component in the extinction law, due to a larger fraction of large grains. The extra large grains are most likely ices from supernova ejecta and will significantly alter the extinction properties of the region until they sublime in 50 – 100 Myr. We discuss the implications of this extinction law for the Tarantula nebula and in general for regions of massive star formation in galaxies. Our results suggest that fluxes of strongly star forming regions are likely to be underestimated by a factor of about 2 in the optical.

**Key words:** Hertzsprung–Russell and colour–magnitude diagrams — dust, extinction — Magellanic Clouds

## 1 INTRODUCTION

The Hubble Tarantula Treasury Project (HTTP) is a photometric survey at high spatial resolution of the Tarantula nebula (30 Dor), from near ultraviolet (NUV) to near infrared (NIR) wavelengths (Sabbi et al. 2013). Its purpose is to reconstruct the region’s star-formation history in space and time on a parsec scale over a total extent of  $\sim 240 \times 190 \text{ pc}^2$ . The ultimate goal is to establish the strength, duration, and spatial scale of the star-formation episodes and their possible mutual relationships. An initial study limited to the central NGC 2070 cluster (Cignoni et al. 2015) confirms that over the past  $\sim 20$  Myr the cluster experienced a prolonged activ-

ity of star formation (e.g., Walborn & Blades 1997; Walborn et al. 1999), with several episodes (De Marchi et al. 2011a), culminating in a peak  $\sim 1 - 3$  Myr ago.

Besides high-quality photometry (Sabbi et al. 2015), these studies rely on our ability to securely measure the intrinsic physical properties of stars, i.e. their true colours and luminosities, since these are crucial to extract reliable masses, ages and other physical parameters to track the star-formation process. Knowledge of the properties and amount of the interstellar extinction is thus of paramount importance, and equally fundamental is knowing how to apply this information to correct the photometry of individual stars. This is particularly crucial in an environment such as the Tarantula nebula, due to its complex structure and to the presence of a considerable amount of atomic and molecular gas (e.g., Indebetouw et al. 2013; Yeh et al. 2015) and dust (e.g., Meixner et al. 2013), resulting in a patchy and uneven level of extinction across the nebula.

<sup>\*</sup> Based on observations with the NASA/ESA *Hubble Space Telescope*, obtained at the Space Telescope Science Institute, which is operated by AURA, Inc., under NASA contract NAS5-26555.

High resolution *Hubble Space Telescope* (HST) studies of the massive stellar Tarantula clusters NGC 2070 and Hodge 301 have long shown a wide spread of extinction values (e.g., Hunter et al. 1995a; Grebel & Chu 2000; De Marchi et al. 2011a), particularly in the central NGC 2070 cluster, where  $A_V$  varies by more than 3 mag over regions of  $\sim 40$  pc across, as shown by Maíz Apellániz et al. (2014) and De Marchi & Panagia (2014). More importantly, both Maíz Apellániz et al. (2014) and De Marchi & Panagia (2014) have independently shown from spectroscopy and photometry that the extinction law for the central NGC 2070 cluster is very different from that typical of the diffuse Galactic interstellar medium (ISM), with a  $\sim 50\%$  higher ratio of total-to-selective extinction, namely  $R_V = A_V/E(B - V) = 4.5$  instead of 3.1.

This finding is particularly intriguing because the Tarantula nebula is routinely considered an ideal test case (the “Starburst Rosetta”, Walborn 1991) for regions of strong star formation at greater distances, where observations cannot reveal individual objects and one must rely on integrated properties. Therefore, understanding whether these apparently anomalous extinction properties are just peculiar to the central NGC 2070 cluster or are a common feature throughout the Tarantula complex is fundamental for our understanding and interpretation of the integrated star formation diagnostics and of the chemical evolution in more distant galaxies.

In this paper, we extend the work of De Marchi & Panagia (2014) to the entire Tarantula nebula. The traditional approach to determine the extinction properties is the “pair method”, whereby the spectrum of a reddened star is compared with that of a reference, un-extinguished object of the same spectral type (e.g., Johnson 1968; Massa, Savage & Fitzpatrick 1983; Cardelli, Sembach & Mathis 1992). This requires high quality spectra, extending from the NUV to the NIR, that are difficult to obtain in the crowded 30 Dor regions and are necessarily limited to the brightest and hence most massive stars (e.g., Fitzpatrick & Savage 1984; Gordon et al. 2003; Maíz Apellániz et al. 2014). Following this method results in a sparse coverage of the Tarantula nebula, preferentially limited to the areas of more recent star formation. Conversely, by making use of multi-band photometry of red giant stars in the red clump (RC) phase (e.g., Paczynski & Stanek 1998; Cole 1998; Girardi et al. 1998; Gao et al. 2009; Wang et al. 2013), the method developed by De Marchi & Panagia (2014; see also De Marchi, Panagia & Girardi 2014) allows us to obtain a rich and uniform coverage spread over several thousand lines of sight in the Tarantula region, resulting in a self-consistent absolute extinction curve of high statistical significance over the entire field and wavelength range of the observations.

The structure of the paper is as follows. In Section 2 we describe the HTTP observations relevant for this study. Section 3 is devoted to the identification of RC stars through an innovative use of unsharp-masking techniques. In Section 4 we derive the absolute extinction towards RC stars and the corresponding extinction law. In Section 5 we present the reddening distribution in this field and discuss how this information should be used to correct the photometry of individual objects. A summary and our conclusions follow in Section 6.

## 2 OBSERVATIONS

The observations are part of the HTTP survey, described in detail in Sabbi et al. (2013, 2015). They cover a region of  $16' \times 13'$  including the 30 Dor nebula, corresponding to  $\sim 240 \times 190$  pc<sup>2</sup> at the distance of the Large Magellanic Cloud (LMC). Throughout this paper we

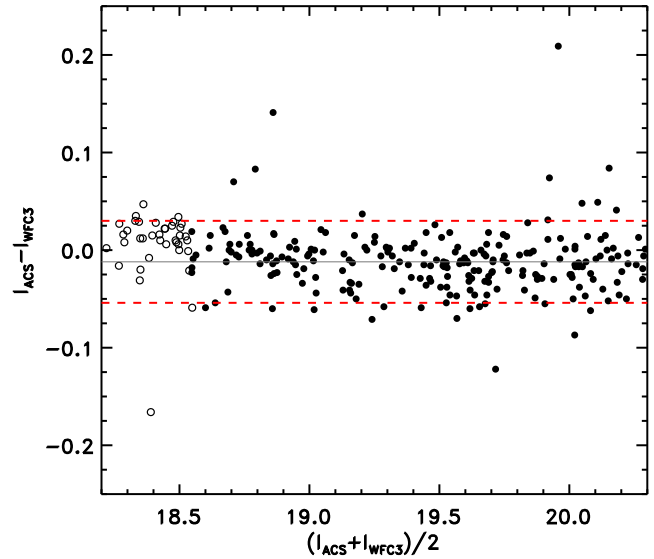


**Figure 1.** Comparison between the  $m_{775}$  magnitudes measured for the same stars with the ACS and WFC3. The mean magnitude difference (solid line) is 0.006 mag, or less than half the typical photometric uncertainty of 0.014 mag ( $1\sigma$ ). The dashed lines mark the  $\pm 3\sigma$  band.

will adopt a distance modulus  $(m - M)_0 = 18.55 \pm 0.05$  as obtained by Panagia et al. (1991; see also Panagia 2005) for SN 1987A, located in the vicinity of the Tarantula nebula. The observations were obtained with the *Advanced Camera for Surveys* (ACS) and *Wide Field Camera 3* (WFC3) instruments on board the *HST* in a set of broad and narrow bands over the range  $0.27 - 1.6 \mu\text{m}$  (respectively F275W, F336W, F555W, F658N, F775W, F110W, and F160W). The photometric reduction and the corresponding catalogue are presented in Sabbi et al. (2015). That paper also illustrates how the two cameras were used to cover the entire field and it provides a detailed list of the exposure times reached in each field. The latter typically amount to 1 164 s in the F275W band, 1 402 s in F336W, 2 270 s in F555W, 2 220 s in F658N, 2 329 s or 2 639 s in F775W, 1 298 s in F110W, and 1 598 s in F160W

Observations in the F775W band were taken with both the ACS and WFC3, covering adjacent regions (see Sabbi et al. 2015 for details). Both cameras feature a filter with that name, but although rather similar their overall response in those bands is not quite the same. In Figure 1, we show the differences between the F775W magnitudes of objects in a strip of  $\sim 16' \times 1'$  that was observed in this band with both cameras. The selected magnitude range,  $18 \lesssim m_{775} \lesssim 20$ , is relevant for the RC stars discussed in this work. The thin solid line shows the mean magnitude difference between the two bands, corresponding to 0.006 mag. The difference is smaller than the typical photometric uncertainty for these objects, namely  $\sim 0.014$  mag (the dashed lines mark the corresponding  $\pm 3\sigma$  band). The root mean square deviation with respect to the mean is 0.038 mag, whereas the same root mean square deviation with respect to zero is just a millimagnitude larger, or 0.039 mag, making a correction not necessary.

Close inspection of the trend seen in the figure might suggest that there is a small colour term, since for this population the magnitude correlates directly with the colour. However, most of the stars in the range  $\sim 18.2 - 18.6$  have uncertainties estimated by Sabbi et al. (2015) to be 0.1 mag due to saturation (open circles in Figure 1). For this reason, the apparent deviation is not significant. Indeed, as we will show in Section 4, there is no detectable system-

**Table 1.** Apparent magnitudes  $m_{\text{RC}}$  of the RC and corresponding  $1\sigma$  spread in all bands, already including the effects of the distance and extinction by intervening MW dust in the foreground.

Band	$m_{\text{RC}}$	$\sigma$
F275W	22.20	0.12
F336W	20.34	0.12
F438W	19.98	0.10
F555W	19.16	0.08
F775W	18.21	0.08
F110W	17.72	0.10
F160W	17.15	0.10

atic difference between the slopes of the reddening vectors in the northern and southern portions of the field, covered respectively by the WFC 3 and ACS. Therefore, in the context of this work it is not necessary to apply a colour-term correction to the photometry and in the following we will not distinguish between the two F775W bands.

Note that in Figure 1 there are a few stars with differences exceeding  $3\sigma$  (dashed lines). Even though their number is not statistically significant, these objects could be variable stars in the field, and the magnitude difference may originate because the ACS and WFC3 observations were not taken simultaneously, or they might be blends or stars with nearby neighbours in projection.

Selecting from the Sabbi et al. (2015) catalogue all the stars with combined photometric uncertainty  $\leq 0.1$  mag in the F555W and F775W bands ( $\sim 755\,000$  objects), we obtain the colour-magnitude diagram (CMD) shown in Figure 2. Following Romaniello (1998), the combined uncertainty  $\delta_2$  is defined as:

$$\delta_2 = \sqrt{\frac{\delta_{555}^2 + \delta_{775}^2}{2}} \quad (1)$$

where  $\delta_{555}$  and  $\delta_{775}$  are the uncertainties in each individual band.<sup>1</sup>

Besides a rather broad upper main sequence (UMS), several times wider than the photometric uncertainty  $\delta_2 < 0.1$  mag, the most prominent feature of Figure 2 is an elongated stellar sequence almost parallel to the main sequence (MS) itself but well separated from it. To help characterise its nature, we show as a red circle the location of the “nominal RC”, defined as the theoretical RC of stars of the lowest metallicity applicable to this field and for ages in the range 1.4 – 3.0 Gyr. De Marchi, Panagia & Girardi (2014) have shown that a metallicity  $Z = 0.004$  is appropriate for the old stars ( $> 1$  Gyr) in 30 Dor.

The apparent magnitudes of the nominal RC and the  $1\sigma$  spread around them are listed in Table 1 for the bands relevant to this study (derived from De Marchi et al. 2014; De Marchi & Panagia 2014). These magnitudes take account of the distance modulus  $(m - M)_0 = 18.55$  (Panagia et al. 1991; Panagia 2005; Walborn & Blades 1997) and already include the contribution of the foreground Milky Way (MW) absorption along the line of sight. Fitzpatrick & Savage (1984) estimated the latter to be  $E(B - V) = 0.07$  or  $A_V = 0.22$  and these are the values that we will assume throughout this work.

The excellent agreement between the position of the nominal RC and the head of the elongated sequence confirms that the latter

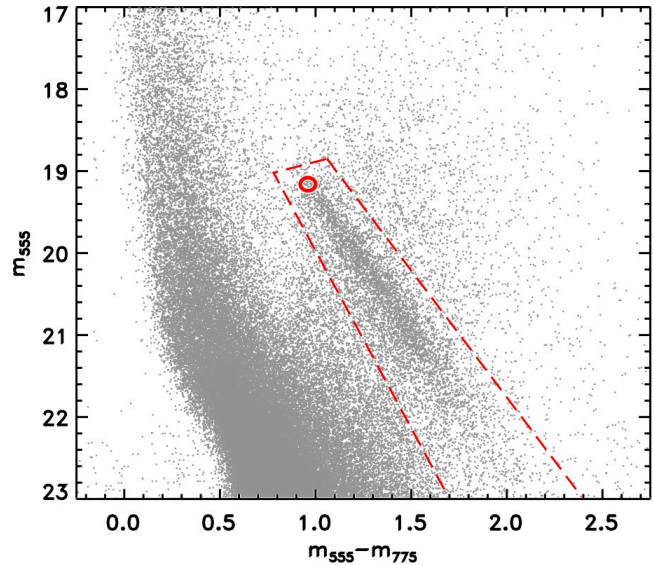


**Figure 2.** CMD of the entire field. The rather broad UMS suggests the presence of considerable and uneven level of extinction in the field. This is confirmed by the prominent RC, extending by several magnitudes from its expected location (red circle).

is indeed made up of RC stars, which are displaced in the CMD along the direction of the reddening vector by the considerable and uneven levels of extinction present in this field. The extended RC has been used in the past to study the reddening distribution and to derive reddening maps in the Magellanic clouds, having assumed an extinction law (e.g. Zaritsky 1999; Haschke, Grebel & Duffau 2011; Tatton et al. 2013). More recently, De Marchi et al. (2014) and De Marchi & Panagia (2014) have shown how to use the extended RC feature in CMDs like that of Figure 2 to derive the extinction law and the extinction to the individual objects in the field. The procedure includes three main steps, namely, *i*) the identification of the candidate RC stars, *ii*) the removal of possible outliers, and *iii*) the determination of the slope of the reddening vector in each set of bands. In general, in order to identify candidate RC stars one needs to know from theory the intrinsic colour and magnitude of the nominal RC, for the metallicity and distance of the population under study (see e.g. Table 1). However, when the RC population consists of several thousands stars, like in the present case, we can follow a fully empirical approach and determine the location of the un-extinguished RC in the CMD using on it the image sharpening technique known as “unsharp masking.”

### 3 UNSHARP MASKING

The technique of unsharp-masking photographic images was originally presented by Spiegler & Juris (1931) and later discussed by Yule (1944). It consists in making an image sharper by overlapping the image itself and an inverted blurred version of it. The blurred image is an out of focus version of the original and has to be subtracted from it (hence it is printed in negative if the original is in positive, or vice-versa). The blurred reversed duplicate is called a mask. Combining the mask with the original image reduces considerably the intensity of the low frequency features, but does not affect the high frequency contrast. Therefore, the image appears sharper because of the enhancement in the high frequency features.

Photographic masking as a technique was regularly used in the

<sup>1</sup> The definition given by Equation 1 can be generalised for any combination of bands.

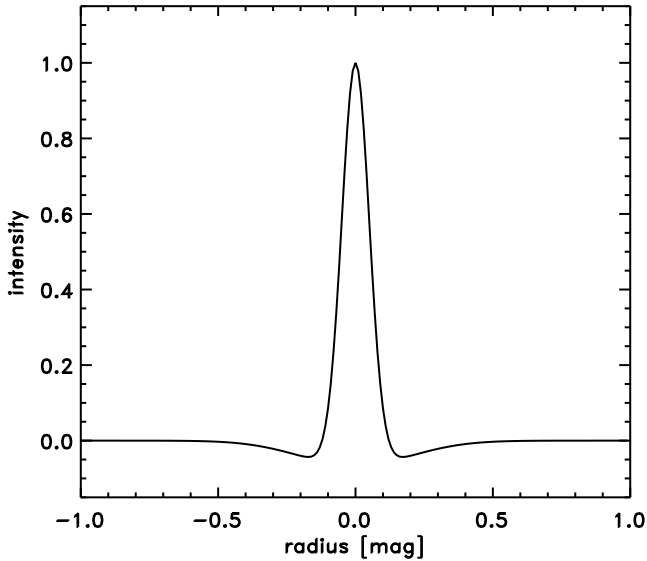


**Figure 3.** Profile of the kernel used for unsharp-masking the CMD of Figure 2.

graphic arts industry. Its principle is today routinely applied in the unsharp-masking tools of modern digital-imaging software packages, such as *GIMP* (Kylander & Kylander 1999). The software subtracts from the original a Gaussian-blurred copy of it. Conceptually, digital unsharp-masking is equivalent to the linear operation of convolving the original with a kernel that is the Dirac delta minus a Gaussian blur kernel.

In this work we use unsharp masking in an innovative way, by applying it to the CMDs, rather than to the digital images themselves. First the CMD is converted to an image, i.e. a two-dimensional array similar to a Hess diagram (Hess 1924). The points in the CMD are mapped onto an array with a sampling of 0.01 mag in colour and magnitude and the array is then convolved with a narrow Gaussian beam. The convolution is meant to assign to each CMD point the proper resolution, including uncertainties on the photometry and on the nature of the objects, as if it were the resolution element of an image. With a typical photometric uncertainty of  $\sim 0.025$  mag for the stars in the CMD of Figure 2, we have used  $\sigma = 0.05$  mag, or twice the photometric uncertainty. The second step is the creation of the mask, by convolving the resulting CMD image with a wider Gaussian beam. We have experimented with several values and selected  $\sigma = 0.2$  mag, although values in the range  $0.15 < \sigma < 0.30$  mag would give comparably good results. The mask is then subtracted from the CMD image. Note that, analytically, these operations are equivalent to convolving the CMD with a kernel. Instead of a Dirac delta minus a Gaussian beam, our kernel is the difference between two Gaussian beams with different  $\sigma$ . A radial section of the resulting kernel is shown in Figure 3.

Application of the unsharp-masking kernel to the CMD results in an improved definition of local density enhancements, such as the elongated RC sequence or the sub-structures along the UMS (see Figure 4). These features were already present in Figure 2, but they were harder to distinguish and characterise quantitatively due to the high density of more uniformly distributed objects around them. By reducing the contrast of the low-frequency component in the CMD (i.e. of the points more uniformly distributed), unsharp masking makes it easier to identify high-frequency structures otherwise overwhelmed in the background. The location of these overdensities in the CMD is crucial to identify the parameter

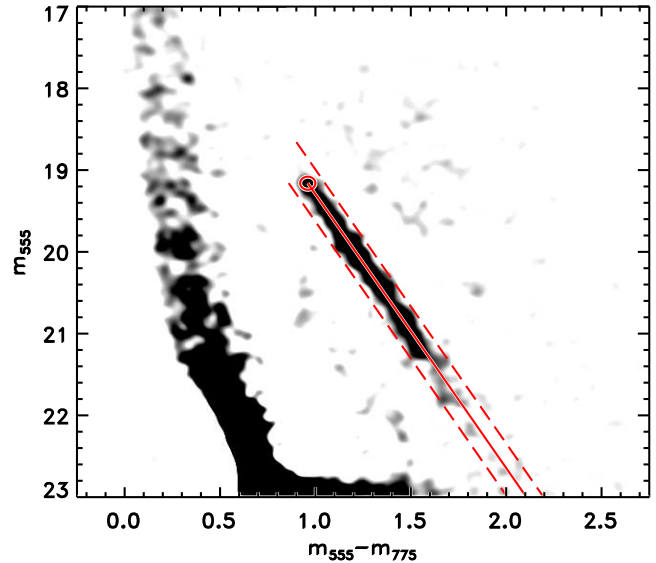


**Figure 4.** Same CMD as in Figure 2 after unsharp masking. The solid line traces the ridge along the elongated RC, while the ellipse corresponds to the expected location of the un-extinguished RC. The dashed lines define an envelope to the distribution of RC stars in the CMD (see Section 5).

space defined by objects sharing a common evolutionary phase. Although it is not possible to identify which individual objects are in that specific evolutionary phase because there are potentially also other stars in that region of the CMD, knowing where the objects are located in the parameter space of the CMD provides critical constraints to stellar evolution.

An example of the local overdensities are the knots seen along the UMS, particularly in the range  $20 \lesssim V \lesssim 21$ , which correspond to multiple turn-on points where pre-main sequence (PMS) stars reach the MS (Hunter et al. 1995b; Sirianni et al. 2000; Brandner et al. 2001; Cignoni et al. 2010), suggesting the existence of separate generations of stars in the field (see De Marchi et al. 2011a; Cignoni et al. 2015). Another example are the knots seen along the elongated RC sequence, indicating that the density distribution of the ISM is not uniform and that major, discrete structures are present in the field as well as along the line of sight. We will discuss these findings in detail in a forthcoming paper (Panagia & De Marchi, in preparation).

As regards the elongated distribution of RC stars, unsharp masking allows us to derive very accurately its ridge line, as shown in Figure 4. Consequently, we can easily determine the direction of the reddening vector. No prior knowledge of the location of the un-extinguished RC is needed, since the head of the distribution empirically defines the un-extinguished RC. In fact, the figure shows that there is an excellent match between the observed head of the elongated RC sequence and the theoretical un-extinguished RC (ellipse). This confirms the validity of the parameter set that we had assumed, namely the theoretical models of the RC (Girardi & Salaris 2001; Salaris & Girardi 2002), the value of the foreground extinction (Fitzpatrick & Savage 1984) and the distance modulus (Panagia et al. 1991; Panagia 2005). These parameters are independent of one another and independent of the measurements, so the good match seen in Figure 4 confirms the appropriateness of the adopted values.

As mentioned above, it is important to remove from the CMD of Figure 2 possible outliers that are present in the region of the extended RC without being RC stars. This is likely the case of

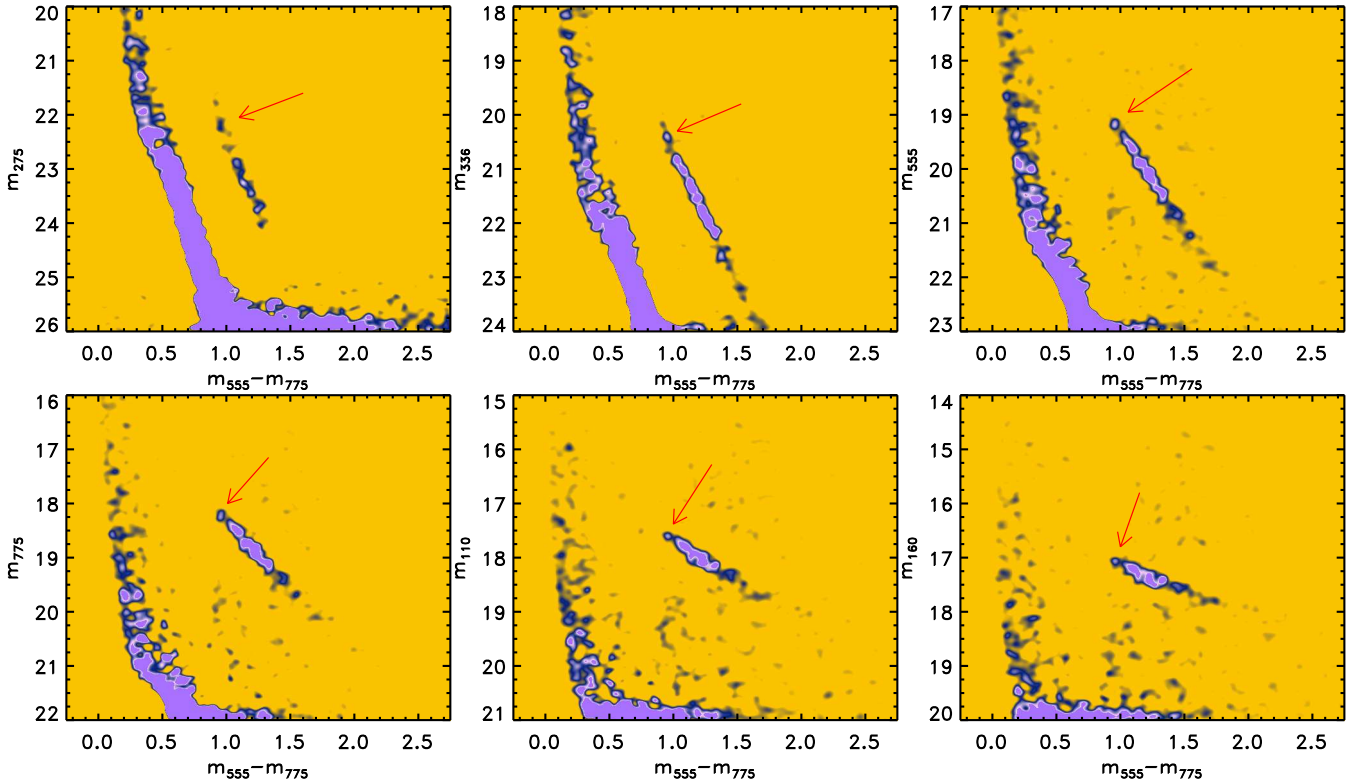


**Figure 5.** Unsharp masking applied to all CMDs clearly reveals the location of the un-extinguished RC, indicated by the arrows. The slope of the reddening vector in all bands is obtained through a linear fit to the elongated RC.

the very young PMS stars, whose broad-band colours could place them in that CMD region. PMS objects are known to populate in large amounts the core of 30 Dor (e.g. De Marchi et al. 2011a), and are easily identified through their  $H\alpha$  excess emission following the method described by De Marchi, Panagia & Romaniello (2010) and De Marchi et al. (2011b). Therefore, before applying unsharp masking to the CMD of Figure 2, we have removed from the region inside the dashed lines about 1% of the stars, since they have  $H\alpha$  equivalent width  $W_{\text{eq}}(H\alpha) > 3 \text{ \AA}$  and could be PMS stars (White & Basri 2003). The fraction is very small because, according to models of PMS stars (e.g. Tognelli, Degl’Innocenti & Prada Moroni 2012), only objects younger than  $\sim 0.25$  Myr may be found in that region of the CMD.

## 4 THE EXTINCTION LAW AND ITS PROPERTIES

### 4.1 Deriving the extinction law

From the CMDs shown in Figure 5, we derived the slope of the reddening vector in all bands, as a function of the  $m_{555} - m_{775}$  colour. These slopes are in fact the ratio  $R$  of absolute ( $A$ ) and selective ( $E$ ) extinction in the specific bands. To derive an accurate measure of  $R$  in each diagram, we used a linear fit along the extended RC, with weights proportional to the density of objects in the CMD after unsharp masking. The values of  $R$  and corresponding uncertainties are listed in Table 2 for various areas across the field. In addition to the full  $16' \times 13'$  region, we have measured the values of  $R$  separately in the northern and southern half fields, as well as in the four quadrants.

As for the uncertainties, the values listed in Table 2 correspond to the dispersion around the best fit. Formally, the uncertainty on

the mean is a factor  $\sqrt{N}$  smaller, where  $N$  is the number of stars along the extended RC between the dashed lines in Figure 4, which amounts to  $\sim 3500$  objects over the whole field. Therefore, the formal uncertainties on  $R$  are typically less than 0.5%. However, this would be fully correct only if the filters were monochromatic and if the properties of the grains were the same everywhere. In fact, the filters are broad bands and, as we will show, small variations in the reddening slopes suggest slight differences in the grain properties. Even though these differences are small, they indicate that the extinction law is not exactly the same across the area and, therefore, we cannot take advantage of the statistics because the dispersion is not only due to observational uncertainties. Hence, we quote the root-mean-square uncertainties listed in Table 2 since they represent the actual extent of the dispersion.

Note that the systematically larger uncertainties on the slope  $R$  in the F275W band are due to the considerably shorter exposure times and the “red leak” affecting this band (see Sabbi et al. 2015 and Dressel 2015 for details).

Within the formal uncertainties listed in Table 2, the slopes  $R$  in the four quadrants are in agreement with one another. There is, however, a small systematic variation in the SE quadrant, where  $R$  is always lower than in the rest of the field, by about 12%. The origin of this small difference will be discussed in more detail in a future work (De Marchi, Panagia, et al. 2015, in preparation), but it is likely related to the smaller fraction of large grains in this region, compared to the rest of the field. What is particularly remarkable, however, is the linearity of the extinction feature seen in all panels of Figure 5. If the properties of the grains were changing with the environment, one would expect that they should be very different in regions of high and low extinction, but this is not what Figure 5 suggests. We will discuss this in detail in a future paper (De Marchi,

**Table 2.** Values of the ratio  $R$  between absolute ( $A$ ) and selective ( $E$ ) extinction across the field of our observations, with the corresponding uncertainties. The effective wavelength ( $\lambda$ ) and wave number ( $1/\lambda$ ) of each band are also indicated.

(1)	(2)	(3)	(4)	(5)	(6)	(7)	(8)	(9)	(10)
Band combination	$\lambda$ [Å]	$1/\lambda$ [ $\mu\text{m}^{-1}$ ]	$R$ Whole field	$R$ North	$R$ South	$R$ Northeast	$R$ Northwest	$R$ Southeast	$R$ Southwest
$A_{275}/E(m_{555} - m_{775})$	2 712	3.69	$5.15 \pm 0.38$	$5.15 \pm 0.49$	$5.12 \pm 0.55$	$5.07 \pm 1.01$	$4.96 \pm 0.86$	$4.71 \pm 0.56$	$5.11 \pm 0.79$
$A_{336}/E(m_{555} - m_{775})$	3 356	2.98	$4.79 \pm 0.19$	$4.92 \pm 0.29$	$4.69 \pm 0.23$	$5.00 \pm 0.38$	$4.82 \pm 0.47$	$4.55 \pm 0.40$	$4.81 \pm 0.38$
$A_{555}/E(m_{555} - m_{775})$	5 322	1.88	$3.35 \pm 0.15$	$3.44 \pm 0.21$	$3.20 \pm 0.19$	$3.47 \pm 0.14$	$3.41 \pm 0.36$	$3.12 \pm 0.32$	$3.28 \pm 0.34$
$A_{775}/E(m_{555} - m_{775})$	7 680	1.30	$2.26 \pm 0.14$	$2.44 \pm 0.19$	$2.12 \pm 0.17$	$2.47 \pm 0.38$	$2.41 \pm 0.31$	$2.03 \pm 0.30$	$2.20 \pm 0.34$
$A_{110}/E(m_{555} - m_{775})$	11 608	0.86	$1.41 \pm 0.15$	$1.54 \pm 0.18$	$1.26 \pm 0.19$	$1.59 \pm 0.33$	$1.52 \pm 0.34$	$1.23 \pm 0.30$	$1.30 \pm 0.43$
$A_{160}/E(m_{555} - m_{775})$	15 387	0.65	$0.95 \pm 0.18$	$0.98 \pm 0.24$	$0.90 \pm 0.22$	$1.00 \pm 0.49$	$0.98 \pm 0.40$	$0.89 \pm 0.33$	$0.95 \pm 0.51$

Panagia, et al. 2015, in preparation), but it is already clear that the linearity of the features sets stringent limits on the spatial variation of grain properties.

In the following, we will derive the extinction law for the whole region covered by the HTTP observations from the values listed in Column (4). It is customary to express the extinction law through the ratio

$$R_{BV}(\lambda) \equiv \frac{A(\lambda)}{E(B-V)}, \quad (2)$$

where  $A(\lambda)$  is the extinction in the specific band and  $E(B-V)$  the colour excess in the canonical Johnson  $B$  and  $V$  bands. Since our observations do not include a filter close in wavelength to the Johnson  $B$  band, expressing the  $R$  values of Table 2 as a function of  $E(B-V)$  as required by Equation 2 could result in larger uncertainties. Instead, we will express the extinction law using the standard  $E(V-I)$  colour excess, since our observations include filters very close to these standard Johnson–Cousin bands and interpolation in that case is much more robust. Conversion of the measured values of Table 2 into

$$R_{VI}(\lambda) \equiv \frac{A(\lambda)}{E(V-I)} \quad (3)$$

is easily done through spline interpolation (see De Marchi et al. 2014).

The  $R_{VI}(\lambda)$  values obtained in this way are shown in Figure 6, for the specific wavelengths of our observations. The dots are the values derived for the entire field and the red solid line shows a spline interpolation through the points. As mentioned above, the systematically shorter exposures and the red leak (Dressel 2015) in the F275W band cause a larger uncertainty on the value of  $R_{VI}(\lambda)$  in the near ultraviolet (NUV). For this reason, we have indicated with a dotted line the spline interpolation in that wavelength range.

For easier comparison with previous works, the interpolated  $R_{VI}(\lambda)$  values in the classical Johnson–Cousin bands, at the wavelengths marked by the vertical dotted lines in the figure, are also listed in Table 3. Note that the value for the  $K$  band is actually an extrapolation and, therefore, is indicated in italics in the table. Besides the value of  $R_{VI}(\lambda)$ , in Table 3 we provide for reference also the values of  $R_{BV}(\lambda)$  as per Equation 2, but we stress again that they are less accurate because of the lack of observations near the wavelengths of the  $B$  band, as mentioned above.

**Table 3.** Interpolated values of  $R_\lambda$  for the most common bands, as a function of both  $E(V-I)$  and  $E(B-V)$ . The latter is less accurate because of the lack of  $B$ -band observations in our photometry. The table also gives the effective wavelengths ( $\lambda$ ) and wave numbers ( $1/\lambda$ ) of the filters, the value of  $R_\lambda^{MW}$  for the canonical extinction law in the diffuse Galactic ISM, and the difference between the latter and our measurements. All values are given for the specific monochromatic effective wavelength as indicated, ignoring the width of the filters. The values for the  $K$  band are extrapolated.

Band	$\lambda$ [Å]	$1/\lambda$ [ $\mu\text{m}^{-1}$ ]	$R_{VI}(\lambda)$	$R_{VI}^{MW}(\lambda)$	$R_{VI}^{diff}(\lambda)$
<i>U</i>	3 650	2.74	$4.41 \pm 0.18$	3.61	0.80
<i>B</i>	4 450	2.25	$3.78 \pm 0.15$	3.05	0.73
<i>V</i>	5 510	1.82	$3.09 \pm 0.15$	2.30	0.79
<i>R</i>	6 580	1.52	$2.58 \pm 0.13$	1.78	0.80
<i>I</i>	8 060	1.24	$2.09 \pm 0.17$	1.29	0.79
<i>J</i>	12 200	0.82	$1.26 \pm 0.18$	0.63	0.63
<i>H</i>	16 300	0.61	$0.84 \pm 0.12$	0.40	0.44
<i>K</i>	21 900	0.46	<i><math>0.52 \pm 0.08</math></i>	0.26	<i>0.26</i>

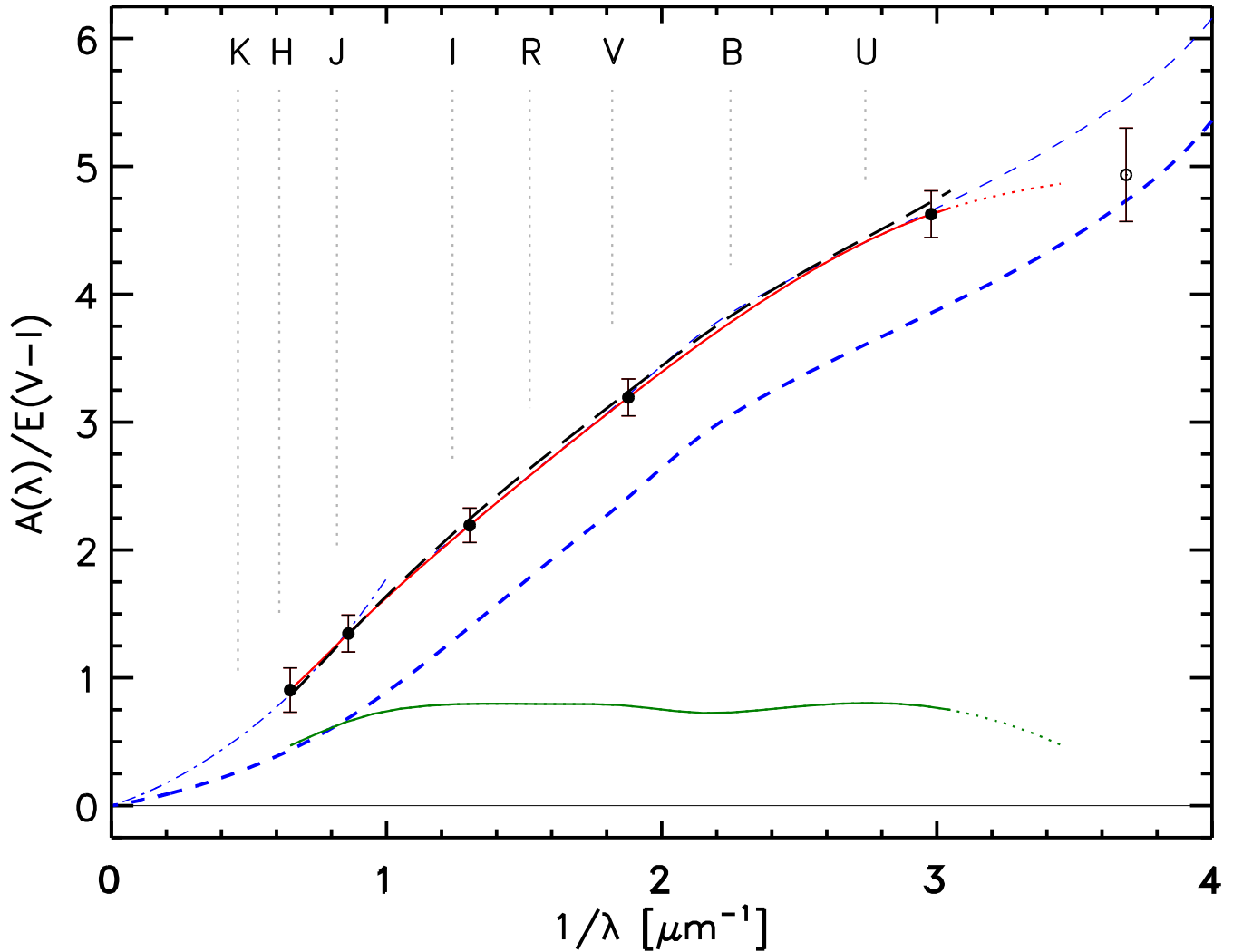
  

Band	$\lambda$ [Å]	$1/\lambda$ [ $\mu\text{m}^{-1}$ ]	$R_{BV}(\lambda)$	$R_{BV}^{MW}(\lambda)$	$R_{BV}^{diff}(\lambda)$
<i>U</i>	3 650	2.74	$6.39 \pm 0.28$	4.75	2.20
<i>B</i>	4 450	2.25	$5.48 \pm 0.24$	4.02	1.93
<i>V</i>	5 510	1.82	$4.48 \pm 0.24$	3.06	1.80
<i>R</i>	6 580	1.52	$3.74 \pm 0.20$	2.35	1.73
<i>I</i>	8 060	1.24	$3.03 \pm 0.26$	1.70	1.58
<i>J</i>	12 200	0.82	$1.83 \pm 0.28$	0.83	0.15
<i>H</i>	16 300	0.61	$1.22 \pm 0.18$	0.53	0.79
<i>K</i>	21 900	0.46	<i><math>0.75 \pm 0.11</math></i>	0.34	<i>0.41</i>

## 4.2 Comparison with previous works

In Figure 6 we also show as a long-dashed line the extinction curve measured by De Marchi & Panagia (2014) with the same method in a smaller region of the Tarantula nebula, namely the central 1'4 radius around R 136. The agreement between the extinction curves over the whole Tarantula field and the R 136 area is very good, over the common wavelength range. This is remarkable because De Marchi & Panagia (2014) covered a much smaller region (sampling only about 140 RC stars instead of the roughly 3 500 objects in this work), and the two studies did not use the exact same set of filters: instead of F775W, De Marchi & Panagia (2014) used F814W. The excellent agreement indicates that the method is solid.

The thick short-dashed line in Figure 6 displays the canoni-



**Figure 6.** Extinction law. The dots show the measurements, with their uncertainties, over the entire  $\sim 16' \times 13'$  field, while the red solid line is a spline interpolation through the values. The uncertainty grows in the NUV domain due to the shallow photometry and filter red leak in the F275W band. The long-dashed line displays the extinction law measured by De Marchi & Panagia (2014) within 1.4 radius of R 136 and is in excellent agreement with that measured in this work over the entire Tarantula nebula. The thick short-dashed line indicates the canonical Galactic extinction law, taken from Fitzpatrick & Massa (1990; see also Fitzpatrick 1999) for  $R_V = 3.1$ , corresponding to  $R_{V_I}(V) = 2.3$ . The thin short-dashed line shows the same law, shortwards of  $\sim 1 \mu\text{m}$  shifted vertically by 0.8 to fit the Tarantula observations in the optical. The dot-dashed line is the Galactic extinction law, longwards  $\sim 1 \mu\text{m}$ , multiplied by a factor of 2 to fit the measured values in the *J* and *H* bands. The green solid line is the difference between the Galactic extinction law (thick short-dashed line) and that of the Tarantula nebula (red solid line).

cal extinction law for the Galactic diffuse ISM, from the work of Fitzpatrick & Massa (1990; see also Fitzpatrick 1999) for  $R_V = R_{BV}(V) = 3.1$ . When expressed in units of  $E(V-I)$ , as per Eq. 3, this corresponds to  $R_{V_I}(V) = 2.3$ , which is a value significantly smaller than the  $R_{V_I}(V) = 3.09 \pm 0.15$  that we measure in the Tarantula (see Table 3).

Gordon et al. (2003) have studied the extinction properties towards eight different lines of sight associated with the LMC 2 Superbubble near the Tarantula nebula. Unfortunately, none of them are included within the field of view of our observations, so it is not possible to make a direct comparison. The closest objects are Sk  $-68^\circ 140$ , located some  $9'$  NE of R 136, and Sk  $-69^\circ 228$ , about  $17'$  SW of it. These and the other more distant lines of sight probed by Gordon et al. (2003) sample regions of considerably more diffuse ISM than those characteristic of the Tarantula nebula itself. It is, therefore, not surprising that the  $R_V$  values measured spec-

troscopically by Gordon et al. (2003) for these stars, e.g.  $R_V = R_{BV}(V) = 3.27 \pm 0.24$  for Sk  $-68^\circ 140$  or  $R_V = R_{BV}(V) = 3.35 \pm 0.33$  for Sk  $-68^\circ 228$ , do not match the value  $R_{BV}(V) = 4.48 \pm 0.17$  measured by De Marchi & Panagia (2014) for the R 136 region and confirmed by these observations for the Tarantula nebula at large. In fact, at optical wavelengths the extinction curve obtained by Gordon et al. (2003) from the LMC 2 Supershell sample is very similar to the Galactic extinction law of Fitzpatrick & Massa (1990; see De Marchi & Panagia 2014 for a direct comparison), which we already concluded does not agree with the extinction curve in the Tarantula (see Figure 6).

Combining HST optical photometry (De Marchi et al. 2011a) with spectroscopy and near-infrared (NIR) photometry from the VLT-FLAMES Tarantula Survey (Evans et al. 2011), Maíz Apellániz et al. (2014) derived the extinction law for the R 136 cluster. Their study of a sample of 83 stars of spectral types O and B



with the Bayesian code CHORIZOS (Maíz Apellániz 2004) concluded that, inside the cluster, the value of  $R_{BV}(V)$  is larger than in the Galactic ISM. They find  $R_{BV}(V) = 4.4 \pm 0.7$  when all 83 objects are considered. Limiting the sample to the 50 objects with the smallest uncertainties, the same average value is found but the spread is reduced, namely,  $R_{BV}(V) = 4.4 \pm 0.4$ . These values are in excellent agreement with those shown in Table 3 for the entire Tarantula nebula.

An immediate implication of our extinction law for the young stars in the Tarantula nebula is that their intrinsic brightness has been so far systematically underestimated. With a median colour excess for UMS stars of  $E(V - I) \simeq 0.5$ , the difference between the Tarantula and Galactic extinction laws implies that one would obtain systematically fainter intrinsic fluxes by a factor of  $\sim 1.5$ , on average, and by more than a factor of 2 for the most extinguished 10% of the stars. As an example, Crowther et al. (2010) derived new luminosities and masses for the most massive members of R 136, correcting their photometry with the extinction law of Fitzpatrick & Savage (1984), namely  $R_{BV}^{30Dor} = 3.7$ . Even approximating this value to 4, as Crowther et al. (2010) have done, the difference with our slope is large ( $R_{BV}^{30Dor} = 4.48 \pm 0.24$ , see Table 3), and implies that the luminosities and masses of the stars are in fact considerably higher than Crowther et al.'s (2010) estimates. For instance, the luminosity of R 136c grows from  $\log L = 6.75$  to  $\log L = 6.9$ , which according to their models brings the mass of the star from  $220 M_{\odot}$  to more than  $300 M_{\odot}$ .

### 4.3 Grain properties

As De Marchi & Panagia (2014) concluded, the extinction law in these regions is “flatter” than in the Galactic ISM, i.e. less steep in logarithmic terms. As one can see from Figure 6, at optical wavelengths in linear terms the extinction law in these regions is almost exactly parallel to the Galactic curve. The thin short-dashed line is the portion of the standard Galactic law shortwards of  $1 \mu\text{m}$  with a vertical offset of 0.8 and it matches the measured extinction curve surprisingly well (the match is in fact so good that the thin short-dashed line is often hard to discern).

The difference between the Galactic extinction law and the one in the Tarantula is shown by the green solid line in Figure 6. At wavelengths shorter than  $\sim 1 \mu\text{m}$  the difference is practically constant (see also Table 3). A noticeable feature is the small dip at  $1/\lambda \simeq 2.2 \mu\text{m}^{-1}$  or  $\lambda \simeq 4550 \mu\text{m}$ , which is a likely consequence of the lack of  $B$ -band observations in our photometry. While the Galactic extinction law features a small knee at this wavelength (see thick short-dashed line), our interpolation is rather smooth in this range since we have no data points between the F336W and F555W filters. Also, we do not regard as significant the apparent decline of the curve in the NUV because of the larger photometric uncertainties and filter red leak at these wavelengths, as mentioned above.

The practically constant difference between the Galactic and Tarantula extinction curves in the optical indicates that the dust is in fact of the same or similar type but that in the Tarantula nebula there is an additional component. Since in the optical the contribution of this component is “grey”, i.e. it does not appear to depend on the wavelength, its most likely origin is the presence of a larger fraction of large grains than in the diffuse ISM in the Galaxy and LMC. This is the accepted interpretation for the high ratios of total-to-selective extinction observed in some Galactic environments (see e.g. Strom, Strom & Yost 1971; Jones 1972; Dunkin & Crawford 1998; Skorzynski, Strobel & Galazutdinov 2003).

The NIR domain provides further indication that, except for the extra grey component, the extinction law in the Tarantula nebula is similar to that of the diffuse ISM in the Galaxy or LMC. At wavelengths longer than  $\sim 1 \mu\text{m}$ , the Tarantula extinction law tapers off as  $\sim \lambda^{-1.7}$ , following almost exactly the observed properties of the Galactic extinction law (e.g. Cardelli, Clayton & Mathis 1989; Wang et al. 2013). The dot-dashed line shown in Figure 6 is the portion of the Galactic extinction law longwards of  $1 \mu\text{m}$  multiplied by a factor of 2, and it offers a remarkably good fit to our observations in the  $J$  and  $H$  bands. Therefore, there is no reason to believe that the nature of the Tarantula grains should be drastically different from that of the diffuse Galactic ISM.

### 4.4 Role of large grains

A detailed analysis of the grain properties as a function of the location inside the nebula will be presented in a forthcoming work (De Marchi, Panagia, et al. 2015, in prep.). However, as De Marchi & Panagia (2014) have already pointed out, simple considerations can provide valuable insights into the properties of the additional dust component present in the 30 Dor regions.

It is well known (e.g., van de Hulst 1957; Greenberg 1968; Draine & Lee 1984) that, at wavelengths short enough, the extinction (= absorption + scattering) cross section of a grain of radius  $a$  tends asymptotically to the geometric cross section  $\sigma_{\text{geom}} = 2\pi a^2$ . At longer wavelengths the cross section is smaller than  $\sigma_{\text{geom}}$  and becomes proportional to the grain volume. Conveniently enough, the transition occurs approximately at  $\lambda_0 \sim 2\pi a$  and, for a given grain size, one would expect a sort of a step function behaviour with the transition occurring rapidly around  $\lambda_0$ . To account for the observed MW extinction law's steady increase with wave number over a wide wavelength range ( $0.2 \mu\text{m} \lesssim \lambda \lesssim 5 \mu\text{m}$ ), it is generally assumed that there is a distribution of grain sizes of the type  $f(a) \propto a^{-\beta}$ , with  $\beta \simeq 3.5$  and the grain radius  $a$  ranging from  $a_{\text{min}} \sim 0.01 \mu\text{m}$  to  $a_{\text{max}} \sim 0.2 \mu\text{m}$  (Mathis, Rumpl & Nordsieck 1977; Draine & Lee 1984).

With  $\beta \simeq 3.5$ , at wavelengths longer than  $2\pi a_{\text{max}}$  the extinction is dominated by the largest grains and is proportional to the total mass in grains. Taking the Galactic extinction law as a reference template, the fact that in the NIR the absolute value of the extinction in the Tarantula is about twice as large as it is in the MW (see Figure 6) implies that the mass fraction in large grains is about twice as high as in the MW. Therefore, the extinction law inside the Tarantula nebula can be represented with the sum of two components: one being the standard Galactic extinction law and the other being made up only of large grains, which are similar in type to those found in the diffuse Galactic ISM.

De Marchi & Panagia (2014) concluded that, for the central regions of 30 Dor, the most likely origin for the higher relative abundance of large grains is the selective injection of “fresh” large grains into the MW mix. The same conclusions can now be extended to the Tarantula nebula at large. The two other ways to explain an excess of large grains would be selective destruction of small grains, or selective condensation of material on the surface of small grains, but both would imply a decrease in the number of small grains and hence an extinction law that is flatter than the MW's at UV wavelengths. In fact, measurements towards the stars of the Magellanic Clouds reveal a steeper rise in the UV extinction curve compared to MW objects (e.g. Fitzpatrick 1998 and references therein). Note that, as mentioned above, the apparent decline of the curve at NUV wavelength in Figure 6 is not significant, due

to the large photometric uncertainties and filter red leak at those wavelengths.

The selective addition of new large grains to the mix can easily account for the presence of the extra grey component in the extinction curve, without conflicting against measurements at other wavelengths. Actually, Gall et al. (2014) recently revealed rapid formation of large,  $\mu\text{m}$ -size dust grains in the dense circumstellar medium around SN 2010jl in the metal-poor galaxy UGC 5189 (Newton & Puckett 2010). Their observations with the *Very Large Telescope* reveal that the extinction curve around the supernova evolves rapidly and turns into a mix of grey-extinction dust grains and MW dust grains. The extinction contribution of the grey dust is about 40% in the  $V$  band. Also in the LMC, recent *Herschel* and *ALMA* observations of SN 1987A (Matsuura et al. 2011; Indebetouw et al. 2014) indicate that a substantial amount ( $> 0.4 M_{\odot}$ ) of large grains ( $> 0.1 \mu\text{m}$ ) is being produced in the ejecta. A similar amount of dust is expected in SN 2010ji if the dust production continues to follow the trend observed so far (Gall et al. 2014). These recent findings make injection of large grains by supernova explosions an exciting possibility for the extinction law in the Tarantula as well. Indeed, very large, grey dust grains recently received much attention in the literature as there is ample evidence for such  $\mu\text{m}$ -sized grains in the Galactic ISM (e.g., Wang, Li & Jiang 2015a).

Star formation has been active for at least 30 Myr in the Tarantula nebula, and possibly longer, as witnessed by the presence of both young and older generations of stars in NGC 2070 (Walborn & Blades 1997; De Marchi et al. 2011a; Cignoni et al. 2015), in Hodge 301 (Grebelt & Chu 2000), and in NGC 2060 (Mignani et al. 2005). If all type II supernova explosions result in an output comparable to that of SN 1987A and SN 2010jl, the excess of large grains should have built up considerably over time and will reach a peak after about  $\sim 50$  Myr, which is the lifetime of the  $8 M_{\odot}$  stars at the lower mass limit of supernova type II progenitors. Even though the large grains are eventually destroyed in the hot gas behind shock fronts in supernova remnants (Draine 2009; Dwek & Scalzo 1980; Dwek 1998), with a total mass in excess of  $10^5 M_{\odot}$  in this starburst region (Bosch et al. 2001; Andersen et al. 2009) the expected supernova rate is above  $10^{-4} \text{yr}^{-1}$  (Cerviño et al. 2001), implying a sustained injection of large grains into the ISM. As an order of magnitude, one would expect in a typical 10 Myr time frame about 1 000 type II SNe, corresponding to up to  $\sim 400 M_{\odot}$  of large grains. With the quoted total mass ( $\sim 10^5 M_{\odot}$ ) and metallicity ( $Z \approx 0.007$ ; e.g. Hill, Andrievsky & Spite 1995; Geha et al. 1998) for these regions, the resulting mass in large grains compares favourably with the expected  $\sim 50\%$  fraction of metals locked in grains (e.g. Savage & Sembach 1996).

To confirm whether this interpretation of the observed extinction law is indeed correct and to understand whether differences with the diffuse Galactic ISM are mainly in the fraction of large grains, further studies are required. Spectroscopic UV observations of early-type stars in suitable locations inside the Tarantula nebula in the range  $\sim 1\,200\text{--}3\,500 \text{\AA}$  are needed to probe the distribution of small grains and to measure in which proportion they are present. These observations are possible with the *Cosmic Origin Spectrograph* (COS) on board the HST.

#### 4.5 Evolution of the extinction properties

So far we have seen that, across the entire Tarantula nebula, the extinction law implies a steeper reddening vector than in the diffuse Galactic ISM: with  $R_V \approx 4.5$ , the reddening vector in the CMDs is consistently  $\sim 50\%$  steeper. Since this is not the case in more

diffuse ISM regions in the LMC, the extinction must be related to the intense star formation witnessed by the Tarantula complex. At the same time, the properties of the extinction law, and hence those of the grains, show relatively small variations across the  $\sim 16' \times 13'$  region that we studied. Indeed, a value of  $R_V \approx 4.5$  is also found in regions devoid of massive stars or in hot X-ray super-bubbles (Wang & Helfand 1991), where  $A_V$  is generally lower (see Sabbi et al. 2015). Therefore, this effect is not limited just to the regions of most recent star formation, but also to those where star formation peaked some 20–30 Myr ago (e.g., Hodge 301 and NGC 2060).

If the overabundance of large grains is due to injection by type II supernovae, as in the case of SN 1987A (Matsuura et al. 2011; Indebetouw et al. 2014) and SN 2010jl (Gall et al. 2014), the ISM enrichment in large grains will be progressive. It will begin with the explosion of the most massive progenitors of the first generation of stars, a few Myr into the star-formation episode, and will continue to increase for about  $\sim 50$  Myr, i.e. the lifetime of the  $8 M_{\odot}$  stars at the lower mass limit of type II progenitors. At this stage, the excess of large grains should be highest and it will begin to decrease progressively as the grains are destroyed in the environment. They must be relatively easy to destroy, since the regions around the Tarantula show a rather standard extinction curve (Gordon et al. 2003). This would be easy to understand if the new large grains were mostly made of ices, which sublime at low temperatures without affecting appreciably the underlying grain distribution. A grey extinction component caused by  $\mu\text{m}$ -size ice grains is also compatible with the mid-IR extinction properties of the Galactic ISM (Wang, Li & Jiang 2015b). Constraints on the timescale of these phenomena can be set by comparing the extinction properties and ages of the populations inside the Tarantula nebula with those in the surrounding regions.

Obviously, our findings can have important implications for the study of the star formation properties in galaxies. Beyond the nearest Universe, star formation properties such as the star formation rate or stellar masses are derived from diagnostics of HII regions (e.g. Kennicutt 1998). Their integrated colours and spectra are dominated by the energy of massive stars and are significantly affected by extinction, i.e. by both the amount and the properties of dust grains. As we have concluded, in regions undergoing massive star formation the properties of the dust grains appear to change from those characteristic of the diffuse Galactic ISM. Even though the changes might be short lived and might last only some  $\sim 50$  Myr, they affect the HII regions when these are most easily detectable in distant galaxies. Therefore, assuming typical ISM conditions in these regions could result in severely inaccurate total masses and star formation rates. If the  $R_V = 4.5$  value measured in the Tarantula nebula is anywhere typical of massive star forming regions and the reddening is high, assuming the classical  $R_V \approx 3$  value could result in fluxes that are about a factor of 2 too faint. The outcome would be a seriously underestimated star formation rate leading to a distorted view of the formation and of the chemical evolution of galaxies (e.g. Matteucci 2012).

## 5 EXTINCTION ACROSS THE TARANTULA NEBULA

In this section we study the reddening distribution across the field in order to derive a reddening map, and discuss how to use it to correct the photometry of individual stars. Having determined the slope of the reddening vector in all observed bands (Table 2), we can measure the total extinction towards objects whose nominal location in the CMD can be determined unambiguously, using them

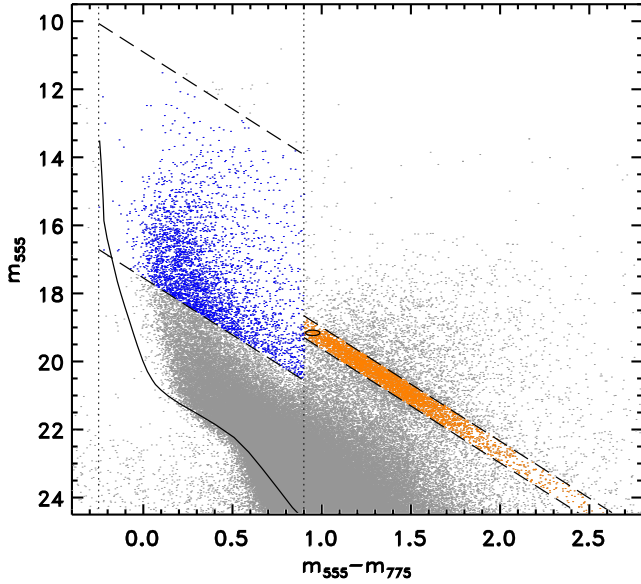


**Figure 7.** The stars used as reddening probes are those between the dashed lines, which are parallel to the direction of the reddening vector in these bands.

as probes of the extinction along their respective lines of sight. These include not only RC stars, but also the objects in the UMS, since that portion of the CMD is not shared with stars in other evolutionary phases.

It is crucial to understand that the extinction map resulting from this collection of lines of sight is by definition a two-dimensional projected distribution. On the other hand, in order to correct the photometry of other objects in the field one would need a three-dimensional distribution, both of the stars and of the absorbing material, to account for their location along the line of sight. One could be tempted to interpolate between lines of sight, but this would not necessarily result in a more accurate photometry. In fact, it is likely to introduce larger uncertainties. As we will show, one has instead to use additional information (e.g. spatial distribution) to determine a meaningful correction for stars other than the reddening probes.

### 5.1 Reddening distribution

The objects serving as reddening probes are those between the dashed lines shown in the CMD of Figure 7. For the RC, we have used as limits the envelopes around the extended RC after unsharp masking (see Figure 4), considering only objects redder than  $m_{555} - m_{775} = 0.9$  since that is the minimum colour consistent with the uncertainty around the nominal RC colour in these bands, taking into account the Galactic extinction component towards the LMC (see Table 1). We have further restricted the selection to stars more massive than  $10 M_{\odot}$  with combined photometric uncertainty  $\delta_2 \leq 0.1$ , and have excluded objects with  $W_{\text{eq}}(H\alpha) > 3 \text{ \AA}$  since they could be PMS stars (see Section 3). In total, about 3 500 objects were selected in this way, corresponding to a projected average RC stars density of  $\sim 20 \text{ arcmin}^{-2}$ . To guarantee a similar density of UMS stars over the same field, we selected a somewhat larger number of objects with colours  $-0.25 < m_{555} - m_{775} < 0.9$ , namely  $\sim 3\,700$ , since many are clustered around R 136. Also in this case, only objects with  $\delta_2 \leq 0.1$  were considered. All stars serving as reddening probes are shown in colour in Figure 7.

For RC stars, the colour excess is calculated as colour difference from  $m_{555} - m_{775} = 0.95$ , i.e. the nominal RC colour in these bands (see Table 1). For UMS stars, however, we use as a reference the isochrone shown in Figure 7, namely the zero age main sequence (ZAMS) from the models of Marigo et al. (2008), extending up to  $60 M_{\odot}$ , and obtained specifically for the HST filters used here and a metallicity of  $Z = 0.007$  as appropriate for 30 Dor and the young LMC population in general (e.g. Hill, Andrievsky & Spite 1995; Geha et al. 1998). We have assumed a distance modulus  $(m - M)_0 = 18.55$  (Panagia et al. 1991; Panagia 2005; Walborn & Blades 1997) and have already included the intervening Galactic extinction along the line of sight, i.e.  $E(B - V) = 0.07$  or  $A_V = 0.22$  as indicated above. Each UMS star is then translated back to the ZAMS, along the direction of the reddening vector, and the colour excess is computed. For stars that, once translated to the isochrone, would be brighter than  $m_{555} = 13.5$  and as such more massive than  $60 M_{\odot}$ , we have assumed an intrinsic colour  $m_{555} - m_{775} = -0.25$ .

Note that most of the UMS stars are likely members of binary systems, so their intrinsic  $m_{555} - m_{775}$  colour can be redder than that of the ZAMS and our procedure could overestimate their reddening. On the other hand, the typical mass ratio for stars above  $\sim 10 M_{\odot}$  like those in our sample is  $q \approx 0.8$  (Kiminki & Kobulnicky 2012; Sana et al. 2012). Model calculations of MS and PMS stars show that for  $q > 0.5$  and an age of 1 Myr or older the  $m_{555} - m_{775}$  colour difference for these massive stars would amount to at most 0.03 mag and as such it can be ignored. Also RC stars could belong to binary systems, but since the nominal RC location is determined from the CMDs after unsharp masking (see Figure 5), the presence of binaries does not affect the colour excess that we derive. In fact, the excellent match between the observed RC location in the CMD and the theoretical models of Girardi & Salaris (2001) indicates that possible lower-mass companions do not appreciably alter the colour of the systems. This is not surprising given the relatively rapid evolution of RC stars along the red giant branch.

The resulting reddening distribution towards the selected stars is shown schematically in Figure 8, panels *b*) and *c*), where the median and the 17 and 83 percentile values of  $A_{555}$  are displayed across the field of view in cells of  $160''$  or  $\sim 40 \text{ pc}$  on a side. For reference, in panel *a*) we mark the positions of the three clusters R 136, Hodge 301, and NGC 2060, as well as the location of the 30 Dor West field studied by De Marchi et al. (2014). Each cell in the panels contains on average  $\sim 110$  stars of either type (RC or UMS), so the percentile values reported in the figure are fully statistically significant, with the exception of some cells along the borders that are only partly covered by the observations. The extent of the shading inside each cell marks the portion actually covered by the observations, and the level of grey in panels *b*) and *c*) reflects the median reddening. The same scale of grey is used in both panels.

The purpose of Figure 8 is to provide a map of the typical  $A_{555}$  values and of their variations across the field, but because of the large dispersions it should not be used as an “extinction map” to correct for reddening the photometry of individual objects. This point is particularly important to understand, because the apparent similarity of the extinction towards RC and UMS stars might be deceiving. Indeed, the median reddening value in fully populated cells and most of those along the borders indicate that there is comparable extinction towards RC and UMS stars inside the same cell. It would, therefore, be tempting to conclude that on the  $\sim 40 \text{ pc}$  scale of a cell the extinction is known and that one might use Figure 8 as a “three-dimensional reddening map” and take the median reddening values to correct the photometry of all stars inside the

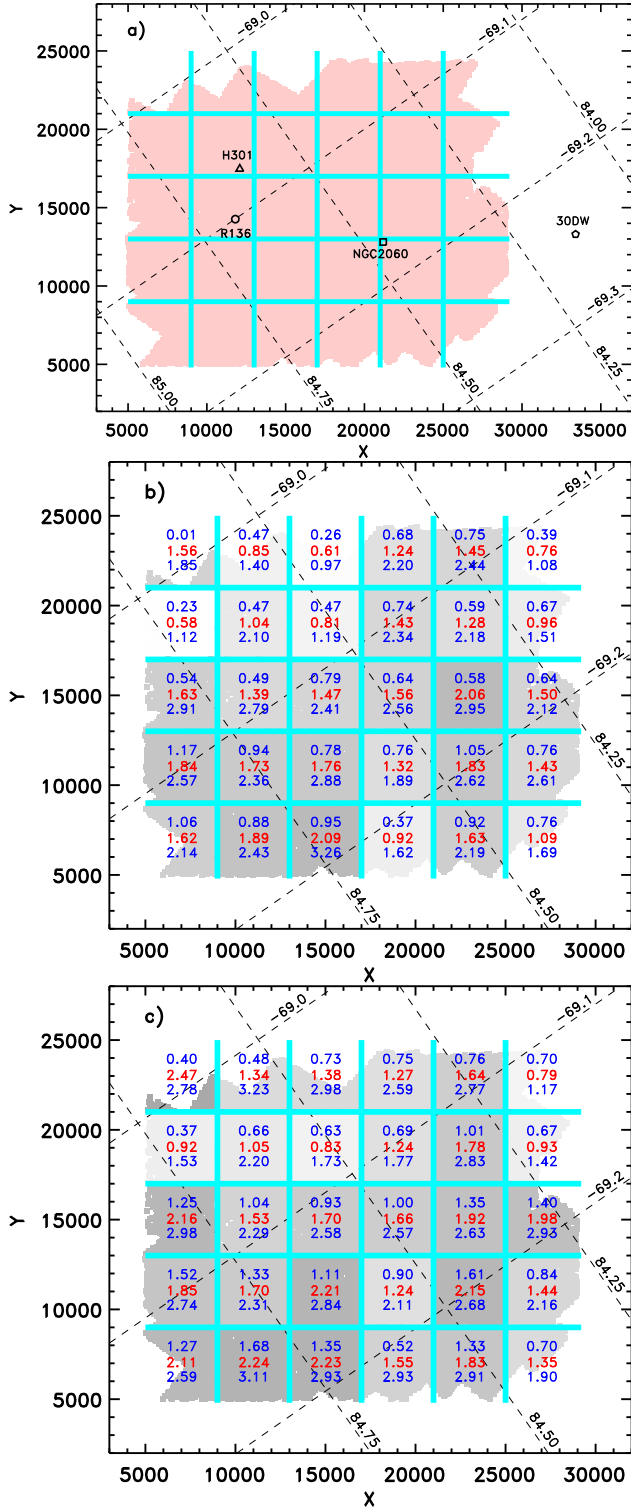


**Figure 8.** Panel *a*): outline of the regions covered by these observations. The centres of the cluster R 136, Hodge 301, and NGC 2060 are marked and we also indicate the 30 Dor West region studied by De Marchi et al. (2014). Panels *b*) and *c*): maps of the reddening statistics towards RC stars and UMS stars, respectively. The entire field of view is divided in cells of  $160''$  or  $\sim 40$  pc on a side. The 17, 50, and 83 percentiles of  $A_{555}$  are displayed in each cell. The extent of the shading inside each cell shows the regions covered by the observations and the level of grey in panels *b*) and *c*) reflects the median reddening value. The same scale of grey is used. Right ascension and declination are shown in decimal degrees.

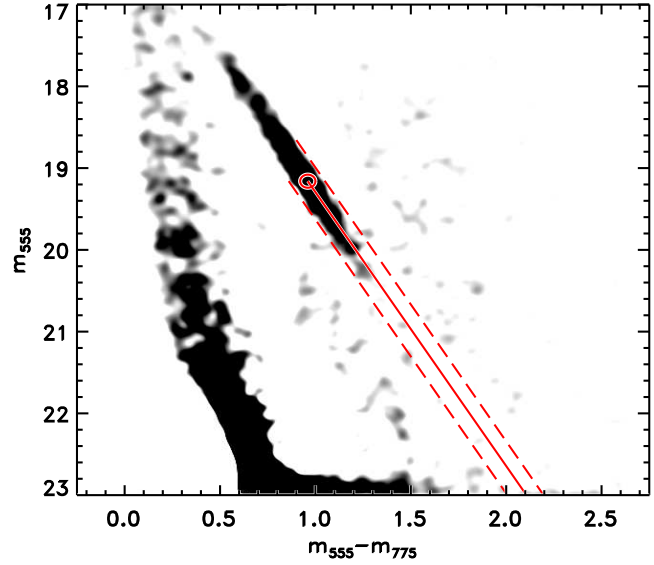


**Figure 9.** Same as Figure 5, but after reddening correction to RC stars only. We have applied to all RC stars inside each cell of Figure 7b the median  $A_{555}$  value pertaining to that cell. Because of the large spread of extinction values inside each cell, applying a single reddening correction to all stars does not bring all RC objects back to their nominal location indicated by the red ellipse.

corresponding cell. As mentioned above, this could introduce large uncertainties, since there are systematic differences in the distribution of reddening values between cells, even if the median values are similar

As a first example, we show in Figure 9 the result of applying to all RC stars inside a cell the median  $A_{555}$  value for that cell. Note that the correction for reddening is applied on purpose only to RC stars, not also to MS objects, so one can directly compare Figure 9 with Figure 4. It is immediately clear that the spread of  $A_{555}$  values inside each cell is so broad that using a single value of  $A_{555}$  for all the RC stars in that cell does not bring them all back to their nominal undispersed location and the spread remains. In other words, without further corrections one would not be able to derive sensible intrinsic physical parameters of RC stars from the CMD of Figure 9, as was the case for Figure 5.

Furthermore, Figure 8 reveals that inside the same cell, RC and UMS stars have very different reddening distributions and it is not possible to use one type of stars to correct for extinction towards the other type. This is immediately clear from Figure 10, offering a direct comparison between the percentile reddening levels measured towards UMS and RC stars. Different colours refer to different levels: blue for 17%, yellow for 50%, and red for 83%. The dots in Figure 10 correspond to the cells as marked in Figure 8. Within  $\pm 0.4$  mag ( $1\sigma$ ; solid lines), there is a fair correlation between the reddening distribution derived from RC and MS stars inside the same cell. This means that, in general, inside a 40 pc-wide cell, the amount of extinction towards RC and UMS stars has a similar distribution, within the quoted  $\pm 0.4$  mag. It is also clear, however, that the reddening towards RC stars begins at systematically lower values than that towards UMS stars, by about 0.4 mag. This is consistent with the projected spatial distribution of RC and UMS stars observed across the region: while RC stars are uniformly distributed, UMS stars are clearly clumped (see Sabbi et al. 2015). This suggests that UMS stars are distributed over a smaller extent also along the line of sight and probe a more limited volume of the

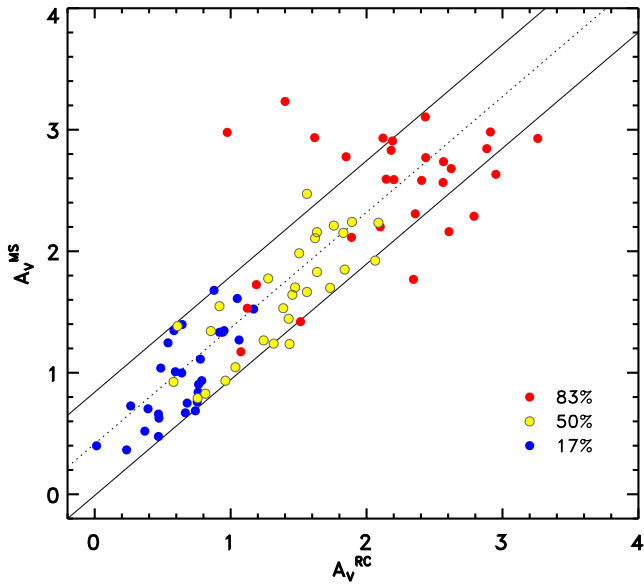


**Figure 10.** Relationship between reddening statistics inside the cells of Figure 8 towards RC and UMS stars. Each dot corresponds to a cell and different colours are used for the 17, 50, and 83 percentile levels. Within  $\pm 0.4$  mag ( $1\sigma$ ; solid lines), there is a fair correlation between the distributions as derived using RC and MS stars.

ISM. This is not surprising, since the young UMS stars tend to be clustered together in more compact groups, while the much older RC stars are distributed more uniformly along the line of sight. For example, in their study of the tomography of the LMC, Haschke, Grebel & Duffau (2012) concluded that young populations (in that work traced by Cepheids) have a considerably smaller extent along the line of sight than older populations.

Figure 10 also reveals that, even inside the same cell, in some cases UMS stars probe systematically more extinguished regions of the ISM, as indicated by the dots in the upper left portion of the figure. It appears that, while the 83 percentile value of the reddening towards RC stars in those cells is in the range  $1 < A_V^{RC} < 2$ , for UMS objects it is  $A_V^{MS} \approx 3$ . A similar conclusion had already been reached by Zaritsky (1999), whose analysis of the reddening distribution towards hot ( $T_{\text{eff}} > 12\,000$  K) and cold ( $5\,500$  K  $< T_{\text{eff}} < 6\,500$  K) stars contained in the Magellanic Clouds Photometric Survey (Harris, Zaritsky & Thompson 1997) revealed that UMS stars are on average more extinguished than red giants. Although this is not always the case, even around the Tarantula nebula (see De Marchi et al. 2014), in comparison to RC objects, UMS stars are by their very nature systematically more closely associated with the higher density ISM regions in which they formed. Therefore, a higher reddening level is to be expected towards UMS objects, particularly when star formation has only recently started. In their study of the main body of the LMC, Zaritsky et al. (2004) concluded indeed that, on average, hot stars appear to be preferentially located in dusty regions.

In summary, our observations leave no doubt that there is a considerable amount of dust distributed between stars along the line of sight in this young complex. It has long been known from radio and IR observations of Galactic star forming regions that distributions of this type are common in the Milky Way (e.g. Panagia 1974; Natta & Panagia 1976; and references therein). It is important to understand whether this is unique to the local Universe or it is typical of massive star forming regions in general, because it ap-

pears to be in contrast with what has been concluded by Calzetti, Kinney & Storchi-Bergmann (1996) for extra-galactic star forming regions. The Tarantula complex offers the best environment to study in detail different phases and conditions of star formation, with no ambiguity about the distance or contamination by background sources.

## 5.2 How to correct for extinction

Although the general trend in Figures 8 and 10 shows that a fair level of correlation exists between the reddening probed by RC and UMS stars, it also reveals that the value of  $A_{555}$  is subject to wide variations over the field. The typical difference between the 17 and 83 percentile values (blue and red dots in Figure 10, respectively) for UMS stars is  $\sim 2.5$  mag, indicating typical fluctuations of the order of  $\pm 1$  mag in  $A_{555}$  ( $1\sigma$ ) towards the young stars inside any given cell. Therefore, using a single value of  $A_{555}$  to correct the photometry of all stars in any given cell will introduce large uncertainties on the stellar parameters ( $L$ ,  $T_{\text{eff}}$ ), with important implications for the masses and ages derived through comparison with theoretical isochrones.

In particular, for a typical PMS star of  $1 M_{\odot}$ , an uncertainty of  $\pm 1$  mag in  $A_V$  leads to an uncertainty of a factor of about 2 on the age and of about 1.5 on the mass, which grows to 2 or more for objects younger than  $\sim 4$  Myr. Such uncertainties dominate over those caused for instance by accretion-induced variability or unresolved binaries (e.g. Gouliermis 2012). Therefore, since one of the goals of the HTTP (Sabbi et al. 2013) is to determine the physical properties of the young populations in these regions (see e.g. Cignoni et al. 2015), including the PMS stars (De Marchi, Panagia et al. 2015, in prep.), it is essential to apply the most appropriate correction for reddening separately on each individual object.

Thus, the simple projected two-dimensional distribution provided by the reddening map (in fact, a higher-resolution version of Figure 8) must be complemented by additional information on the properties and spatial distribution of the objects, in order to constrain the position of the stars with respect to the extinguishing material along the line of sight. In the following, we discuss the conditions under which it is possible to apply an extinction correction to individual young objects in the CMD and how to do it. We can distinguish several cases, as follows.

(i) Massive stars of spectral types O and B (blue dots in Figure 7) spend most of their life on the UMS (e.g., Marigo et al. 2008), so the reddening correction can be determined for each object individually as per the procedure described above, since the extinction law is very robust.

(ii) For young PMS stars that are identified through their  $H\alpha$  excess emission (De Marchi et al. 2010, 2011b) and whose spatial distribution projected on the sky overlaps with that of UMS stars, one can reasonably assume that they are physically co-located with the UMS objects also along the line of sight. In this case, the extinction appropriate for each PMS star can be derived as the average of the extinction towards a subset of UMS stars in their vicinity. For example, this “nearest neighbours” approach has been used to correct for extinction the PMS in the core of 30 Dor (De Marchi et al. 2011a), and in the NGC 346 star forming cluster in the Small Magellanic Cloud (De Marchi et al. 2011b). In both cases, using between 5 and 20 nearest neighbours on the entire photometric catalogue resulted in a tight UMS in the CMD. It is reasonable to adopt this approach also for stars that share the same photometric properties as young PMS objects without necessarily displaying  $H\alpha$  ex-

cess emission, namely objects that occupy a similar position in the broad-band CMD and whose projected spatial distribution follows that of UMS stars. These objects could indeed be PMS stars not actively accreting at the time of observation, as it is known that PMS objects show large variations in their  $H\alpha$  emission over hours or days (e.g. Fernandez et al. 1995; Smith et al. 1999; Alencar et al. 2001).

(iii) For older ( $\gtrsim 10$  Myr) PMS objects with  $H\alpha$  excess emission but with a spatial distribution different from that of UMS stars, it is not safe to assume that the ISM probed by the two types of objects be similar. The UMS stars probe the most recent episode of star formation, associated with a denser ISM, where one would expect higher extinction values than towards older PMS objects. While one could still use the nearest UMS stars to estimate the amount of reddening, it would likely be too high and after correction some stars might appear bluer than the MS. Additional constraints need to be applied in this case. A possible approach, followed for instance by De Marchi et al. (2011a) for the population of  $\sim 12$  Myr old PMS stars in 30 Dor, is to de-redden all these objects by the same amount, chosen in such a way to guarantee a statistically acceptable distribution of colours, i.e. that no more than  $\sim 17\%$  of the objects are bluer than the MS after reddening correction. Alternatively, one could estimate the extinction towards older PMS stars individually using as nearest neighbours the RC objects in their vicinity. As shown above, RC stars are more uniformly distributed and sample a less dense ISM, resulting in typically lower median extinction values towards those lines of sight (see Figures 8 and 10). Needless to say, both approaches imply a larger uncertainty on the physical parameters that one can derive for these PMS objects, and they must be properly taken into account in any further analysis.

(iv) In all other cases, and for a more solid result in case (iii), one needs spectral information. Using large ground-based facilities it is already possible to obtain the spectral type of a sample of bright PMS stars in less crowded regions in the Magellanic Clouds (e.g. Kalari et al. 2014), providing reliable intrinsic colours and effective temperatures for at least the most massive of these objects. In the Magellanic Clouds, it will be possible to extend this investigation to older PMS stars of solar mass with the *James Webb Space Telescope* (Gardner et al. 2006).

Following this approach one obtains a much more reliable extinction correction than the one achievable using pixel-to-pixel maps of the reddening of the gas in the star forming region, estimated from ratios of H recombination lines at different wavelengths (e.g. Natta & Panagia 1984; Calzetti et al. 1996; Pasquali et al. 2011; Pang, Pasquali & Grebel 2011; Zeidler et al. 2015). The reason is easily understood and can be summarised as follows.

(i) A relationship between the colour excess of the gas and the observed and theoretical flux ratio of line pairs can only be defined in the ideal (yet unlikely) case that the dust is all in the foreground and is homogeneously distributed (see Calzetti et al. 1996). If it is not, Natta & Panagia (1984) have shown that the solution is not unique and may span large uncertainties.

(ii) The extinction curve specific to the environment must be known (see Calzetti et al. 1996). As we show in this work, it is not safe to adopt the extinction law of the Galactic diffuse ISM in star forming regions.

(iii) Extinction is the sum of absorption and scattering, which affect light differently depending on whether the photons originate from stars or from an extended gas cloud. While for a star both absorption and scattering result in the loss of a photon from the beam, in a nebula scattering simply diffuses the photon within the nebula

and only absorption will kill it. Therefore, to interpret observed H line intensity ratios properly, a full knowledge of the dust properties including both absorption and scattering cross sections is required.

(iv) The map of gas line ratios is valid for a specific optical depth, that of the gas. Unless stars share a similar location along the line of sight, using these maps for the stars is a delusive strategy and the resulting reddening correction will be systematically wrong.

Since the above conditions are normally not satisfied in massive clusters or regions of extended star formation (and surely not in galaxies; see, e.g., Penner et al. 2015), it is somewhat naïve and exceedingly simplistic to rely on maps of the gas line ratios for a quantitative measure of the reddening towards individual stars. The very fact that the extinction towards the gas is often found to be larger than that of the UMS stars indicates that the thickness of the dust layers in front of stars are not the same as the ones attenuating the gas. Elementary logic dictates that loose matter located behind a source cannot produce reliable, if any, information about what lies in front of that source.

Instead, the approach based on the *nearest neighbours with similar age and spatial distribution* that we describe here provides what is presently the most robust quantitative estimate of the reddening towards individual stars in the Tarantula. Eventually, an even more accurate reddening value for individual stars in the HTTP catalogue is expected to be obtained through a Bayesian study of the spectral energy distribution of individual objects (Arab, Gordon, et al. 2015, in preparation), including stars outside the UMS and RC loci.

## 6 SUMMARY AND CONCLUSIONS

We have studied the properties of the interstellar extinction over a field of  $16' \times 13'$  ( $\sim 240 \times 190$  pc<sup>2</sup>) in the Tarantula nebula, imaged with the *HST* as part of the HTTP (Sabbi et al. 2013). The photometric catalogue contains more than 820 000 stars observed at NUV, optical and NIR wavelengths through the filters F275W, F336W, F555W, F658N, F775W, F110W, and F160W (Sabbi et al. 2015). Since in these regions the levels of extinction are considerable and very uneven, RC stars are found to be spread across the CMD defining a tight band. This has allowed us to accurately derive the absolute extinction  $A(\lambda)$  and the extinction law  $R(\lambda)$  in the range  $\sim 0.3 - 1.6$   $\mu\text{m}$ , from more than 3 500 RC stars. The main results of this work can be summarised as follows.

(i) The CMDs obtained from the observations reveal a prominent elongated sequence, almost parallel to the MS, made up of several thousand RC stars affected by various amounts of extinction (Figure 2). Application of the unsharp-masking kernel to the CMDs reduces the contrast of the low-frequency component, resulting in a vastly improved definition of the sharp, elongated RC feature (Figures 4 and 5).

(ii) From the best linear fit to the elongated RC, we obtain a fully empirical determination of the slopes of the reddening vector in all combinations of bands. The reddening vector appears to have a similar slope over the entire field of view, within the uncertainty, although the SE quadrant of the nebula reveals a systematically lower value of  $R(\lambda)$  by about 12%. The excellent match between the head of the elongated RC sequence and the position of the un-extinguished RC predicted by theoretical models (Girardi & Salaris 2001) is an independent validation of the models.

(iii) The reddening slopes immediately provide the ratio  $R(\lambda)$  of

total-to-selective extinction in the specific *HST* bands, with high accuracy. Knowledge of the un-extinguished position of the RC in the CMDs readily gives the absolute extinction  $A(\lambda)$  in all bands towards more than 3 500 stars. Interpolation at the wavelengths of the standard *B*, *V*, and *I* bands provides the extinction curves in the canonical forms  $R_{BV}(\lambda) \equiv A(\lambda)/E(B - V)$  or  $R_{VI}(\lambda) \equiv A(\lambda)/E(V - I)$  in the range  $\sim 0.3 - 1.6 \mu\text{m}$ . The latter form is more accurate because our photometry includes observations in bands very close to the Johnson–Cousin *V* and *I* filters.

(iv) The slope of the reddening vector in the Tarantula nebula is considerably steeper, in all bands, than in the Galactic diffuse ISM, i.e. the value of  $R$  is systematically higher in 30 Dor (Figure 6) than in the MW. We measure  $R_{BV}(V) = 4.48 \pm 0.24$  and  $R_{VI}(V) = 3.09 \pm 0.15$  instead of the canonical  $R_{BV}(V) = 3.1$  and  $R_{VI}(V) = 2.3$  found in the Galaxy (e.g. Cardelli et al. 1989; Fitzpatrick & Massa 1990). On the other hand, our  $R$  values are in excellent agreement with those measured in the central NGC 2070 cluster by De Marchi & Panagia (2014) from *HST* photometry of RC stars, that is  $R_{BV}(V) = 4.48 \pm 0.17$ , and by Maíz Apellániz et al. (2014) from spectro-photometry of OB-type objects in the same field, namely,  $R_{BV}(V) = 4.4 \pm 0.4$ .

(v) An immediate implication of our extinction law is that the masses derived until now from the photometry of UMS objects have been systematically underestimated, by a factor of  $\sim 1.5$ , on average, and by more than a factor of 2 for the most extinguished 10 % of the stars. For instance, the luminosity of R 136c grows from  $\log L = 6.75$  to  $\log L = 6.9$ , which according to the models of Crowther et al. (2010) brings the star from  $220 M_{\odot}$  to more than  $300 M_{\odot}$ . If the extinction law that we measure in the Tarantula nebula is typical of massive star forming regions in galaxies, current star formation rates of galaxies derived from diagnostics of HII regions will have to be seriously revised upwards.

(vi) At optical wavelengths, the extinction law  $R_{VI}(\lambda)$  is best represented by the Galactic curve shifted vertically by an offset of 0.8. For  $\lambda > 1 \mu\text{m}$ , the best match is the Galactic law multiplied by a factor of 2 (both curves fall off with wavelength as  $\lambda^{-1.7}$ ). We interpret this as indication that the Tarantula extinction curve is due to dust similar to that of the diffuse ISM in the Galaxy, but that it contains a larger fraction of large grains (about a factor of 2). We show that this scenario is consistent with type II supernova explosions injecting “fresh” large grains into an otherwise MW-like mix, as recently revealed by observations of SN 1987A and SN 2010jl. UV observations, e.g. with COS on board the HST, are needed to verify the evolution of the population of grains also at the small end of the size distribution.

(vii) Since these extinction properties are consistently found across the entire Tarantula nebula but not in the more diffuse regions in its surroundings, they must be related to the recent intense star formation episodes inside the nebula itself. Assuming that type II SNe are the source of the extra large grains, their excess should reach a peak after  $\sim 50$  Myr (i.e. the lifetime of the least massive type II SN progenitors), before the grains are destroyed in the environment. The lack of an excess of large grains in the surroundings of the Tarantula suggests that these grains are relatively easy to destroy, making ices in the SNe ejecta their likely source.

(viii) Knowing the slope of the reddening vector for all bands, we can measure the total extinction towards all objects whose nominal CMD location can be determined unambiguously. We select 3 700 UMS objects and 3 500 RC stars to derive uniform, densely populated maps ( $\sim 35$  stars per arcmin<sup>2</sup>) of the extinction towards both young and old objects. Even though there is a fair correlation between RC and UMS reddening over scales of  $\sim 40$  pc, reddening

towards RC stars begins at systematically 0.4 mag lower values and UMS stars have on average 0.4 mag more extinction than RC stars. Not surprisingly, this indicates that UMS objects sample smaller volumes along the line of sight and probe a more limited region of the ISM.

(ix) We address the use of extinction maps for reddening correction in regions of high and variable extinction. We show that it is not sufficient to rely on the projected position of the objects on the sky and that additional information, such as age and spatial distribution, must be used to compensate for the missing knowledge of the line-of-sight distribution of the stars under study. We warn against the large uncertainties inherent in applying extinction corrections based on simple line ratios of the diffuse gas. Instead, an approach based on the nearest RC or UMS neighbours with similar age and spatial distribution provides a more robust quantitative estimate for individual stars.

An important conclusion that we draw from this work is that, in regions of intense star formation, the ISM undergoes fundamental and rapid changes as fresh large grains are selectively injected into it by type II supernovae and are later destroyed. This results in profoundly different extinction properties in these areas for periods of 50 – 100 Myr, with  $R_V$  values in the range 4 – 5 that must be taken into account in the study of cosmological sources. Understanding how these changes correlate with star formation and the timescale on which they proceed in galaxies is fundamental: not only for the study of young resolved stellar populations in nearby galaxies, but also to decipher the properties of star formation and chemical evolution of galaxies in the early Universe.

## ACKNOWLEDGMENTS

We are grateful to an anonymous referee, whose insightful comments have helped us to improve the presentation of this work. Support for HST programme # 12939 was provided by NASA to the US team members through a grant from the Space Telescope Science Institute, which is operated by AURA, Inc., under NASA contract NAS 5–26555. NP acknowledges partial support by STScI–DDRF grant D0001.82435.

## REFERENCES

- Alencar, S., Basri, G., Hartmann, L., Calvet, N. 2005, *A&A*, 440, 595  
 Andersen M., et al., 2009, *ApJ*, 707, 1347  
 Bosch G., Selman F., Melnick J., Terlevich, R., 2001, *A&A*, 380, 137  
 Brandner W., Grebel E., Barbá; R., Walborn N., Moneti A. 2001, *AJ*, 122, 858  
 Calzetti D., Kinney A., Storchi–Bergmann T., 1996, *ApJ*, 458, 132  
 Cardelli J., Clayton G., Mathis J., 1989, *ApJ*, 345, 245  
 Cardelli J., Sembach K., Mathis J., 1992, *AJ*, 104, 1916  
 Cerniño M., et al., 2001, *A&A*, 376, 422  
 Cignoni M., et al., 2010, *ApJ*, 712, L63  
 Cignoni M., et al., 2015, *ApJ*, 811, 76  
 Cole A., 1998, *ApJ*, 500, 137  
 Crowther P., et al., 2010, *MNRAS*, 408, 731  
 De Marchi G., et al., 2011a, *ApJ*, 739, 27  
 De Marchi G., et al., 2011b, *ApJ*, 740, 11  
 De Marchi G., Panagia N., Girardi L., 2014, *MNRAS*, 438, 513  
 De Marchi G., Panagia N., Romaniello M., 2010, *ApJ*, 715, 1  
 De Marchi G., Panagia N., 2014, *MNRAS*, 445, 93  
 Draine, B. 2009, in *Cosmic Dust Near and Far*, ASP Conf. Ser. 414, p. 453  
 Draine B., Lee H., 1984, *ApJ*, 285, 89

- Dressel L., 2015, *Wide Field Camera 3 Instrument Handbook*, (Baltimore: STScI)
- Dunkin S., Crawford I., 1998, *MNRAS*, 298, 275
- Dwek, E. 1998, *ApJ*, 501, 643
- Dwek, E., Scalo, J. 1980, *ApJ*, 239, 193
- Evans C., et al., 2011, *A&A*, 530, A108
- Fernandez, M., Ortiz, E., Eiroa, C., Miranda, L. 1995, *A&AS*, 114, 439
- Fitzpatrick E., 1998, in *Ultraviolet Astrophysics Beyond the IUE Final Archive*, ed. W. Wamsteker, R. Gonzalez Riestra (Noordwijk: ESA), 461
- Fitzpatrick E., 1999, *PASP*, 111, 63
- Fitzpatrick E., Massa D., 1990, *ApJS*, 72, 163
- Fitzpatrick E., Savage B., 1984, *ApJ*, 279, 578
- Gardner J., et al., 2006, *SSRv*, 123, 485
- Gao J., Jiang B., Li A., 2009, *ApJ*, 707, 89
- Gall C., et al., 2014, *Nature*, 511, 326
- Geha M., et al., 1998, *AJ*, 115, 1045
- Girardi L., Groenewegen M., Weiss A., Salaris M., 1998, *MNRAS*, 301, 149
- Girardi L., Salaris M., 2001, *MNRAS*, 323, 109
- Gordon K., Clayton G., Misselt K., Landolt A., Wolff M., 2003, *ApJ*, 594, 279
- Gouliermis D., 2012, *SSRv*, 169, 1
- Grebel E., Chu Y.-H., 2000, *AJ*, 119, 787
- Greenberg J. M., 1968, in *Nebulae and interstellar matter*, ed. B. Middlehurst, L. Aller (Chicago: Univ. Chicago Press), 221
- Harris J., Zaritsky D., Thompson I., 1997, *AJ*, 114, 1933
- Haschke R., Grebel E., Duffau S., 2011, *AJ*, 141, 158
- Haschke R., Grebel E., Duffau S., 2012, *AJ*, 144, 106
- Hess R., 1924, in *Probleme der Astronomie. Festschrift fur Hugo von Seeliger*, (Berlin: Springer), 265.
- Hill V., Andrievsky S., Spite M., 1995, *A&A*, 293, 347
- Hunter D., et al., 1995a, *ApJ*, 444, 758
- Hunter D., et al., 1995b, *ApJ*, 446, 179
- Indebetouw R., et al., 2013, *ApJ*, 774, 73
- Indebetouw R., et al., 2014, *ApJ*, 782, L2
- Johnson H., 1968, in *Nebulae and interstellar matter*, ed. B. Middlehurst, L. Aller (Chicago: Univ. Chicago Press), 167
- Jones B., 1971, *ApJ*, 171, L57
- Kalari V., et al., *A&A*, 564, L7
- Kennicutt R., 1998, *ARA&A*, 36, 189
- Kiminki D., Kobulnicky H., 2012, *ApJ*, 751, 4
- Kylander K., Kylander O., 1999, *GIMP: The official handbook* (Scottsdale: The Coriolis Group)
- Li A., 2009, in *Small Bodies in Planetary Sciences*, Vol. 758, ed. I. Mann, A. Nakamura, T. Mukai (Berlin: Springer), 167
- Maíz Apellániz J., 2004, *PASP*, 116, 859
- Maíz Apellániz J., et al., 2014, *A&A*, 564, A63
- Marigo P., et al., 2008, *A&A*, 482, 883
- Massa D., Savage B., Fitzpatrick E., 1983, *ApJ*, 266, 662
- Mathis J., Rumpl W., Nordsieck K., 1977, *ApJ*, 217, 425
- Matsuura M., et al., 2011, *Sci*, 333, 1258
- Matteucci F., 2012, *Chemical evolution of Galaxies*, (Berlin: Springer)
- Mignani R., et al., 2005, *A&A*, 431, 659
- Natta A., Panagia N., 1976, *A&A*, 50, 191
- Natta A., Panagia N., 1984, *ApJ*, 287, 228
- ] Newton J., Puckett T., 2010, *Central Bureau Electronic Telegrams*, 2532, 1
- Paczynski B., Stanek K., 1998, *ApJ*, 494, L219
- Panagia N., 1974, *ApJ*, 192, 221
- Panagia N., 2005, in *Cosmic Explosions, On the 10<sup>th</sup> Anniversary of SN 1993J*, IAU Coll. 192, ed. J. Marcaide, K. Weiler (Berlin: Springer), 585
- Panagia N., Gilmozzi R., Macchetto F., Adorf H.-M., Kirshner R., 1991, *ApJ*, 380, L23
- Pang X., Pasquali A., Grebel E., 2011, *AJ*, 142, 132
- Pasquali A., et al., 2011, *AJ*, 141, 132
- Penner K., et al., 2015, *ApJ*, submitted (arXiv:1507.0728)
- Sana H., et al., 2012, *Science*, 337, 444
- Sabbi E., et al., 2013, *AJ*, 146, 53
- Sabbi E., et al., 2015, *AJ*, submitted
- Salaris M., Girardi L., 2002, *MNRAS*, 337, 332
- Savage B., Sembach K., 1996, *ARA&A*, 34, 279
- Sirianni M., Nota A., Leitherer C., De Marchi G., Clampin M. 2000, *ApJ*, 533, 203
- Skorzynski W., Strobel A., Galazutdinov G., *A&A*, 408, 297
- Smith, K., Lewis, G., Bonnell, I., Bunclark, P., Emerson, J. 1999, *MNRAS*, 304, 367
- Spiegler G., Juris K., 1931, *Phot. Korr.*, 67, 4
- Strom K., Strom S., Yost J., 1971, *ApJ*, 165, 479
- Tatton B., et al., 2013, *A&A*, 554, A33
- Tognelli E., Degl'Innocenti S., Prada Moroni P. G., 2012, *A&A*, 548, A41
- van de Hulst H., 1957, *Light scattering by small particles*, (New York: Wiley & Sons)
- Walborn N., 1991, in *Massive Stars in Starbursts*, Eds. C. Leitherer, et al. (Cambridge: Cambridge Univ. Press), 145
- Walborn N., et al., 1999, *AJ*, 117, 225
- Walborn N., Blades J., 1997, *ApJS*, 112, 457
- Wang S., Gao J., Jiang B., Li A., Chen, Y., 2013, *ApJ*, 773, 30
- Wang S., Li A., Jiang B., 2015a, *ApJ*, 811, 38
- Wang S., Li A., Jiang B., 2015b, *MNRAS*, 454, 569
- Wang Q., Helfand D., 1991, *ApJ*, 370, 541
- White R., Basri G., 2003, *ApJ*, 582, 1109
- Yeh S., Seaquist E., Matzener C., Pellegrini E., 2015, *ApJ*, 807, 117
- Yule J., 1944, *Phot. J.*, 321
- Zaritsky D., 1999, *AJ*, 118, 2824
- Zaritsky D., Harris J., Thompson I., Grebel E., 2004, *AJ*, 128, 1606
- Zeidler P., et al., 2015, *AJ*, 150, 78